

SIMULATIONS OF HUMAN SWIMMING USING SMOOTHED PARTICLE HYDRODYNAMICS

Raymond C. Z. COHEN^{1*}, Paul W. CLEARY¹ and Bruce MASON²

¹ CSIRO Mathematical and Information Sciences, Clayton, Victoria 3169, AUSTRALIA

² Australian Institute of Sport, Canberra, AUSTRALIA

*Corresponding author, E-mail address: Raymond.Cohen@csiro.au

ABSTRACT

Human swimming is a challenging problem to simulate using computational fluid dynamics because of the combination of turbulent flow; complex free surface motion including splashing and entrainment of gas; and rapidly deforming swimmer geometry. The mesh-free Smoothed Particle Hydrodynamics (SPH) technique is ideally suited to overcome many of these difficulties. Initial simulations of towing using SPH for both male and female swimmers in a fixed glide pose at different speeds are presented. The surface shapes of the swimmers' bodies were generated from laser scans of athletes. The motion of a male swimmer in submerged dolphin-kick swimming is also explored. The stroke kinematics was generated using skeletal based deformation of the surface mesh to closely mimic underwater video footage of an elite swimmer. The two cases investigated are of slow kicking at 0.8 Hz with a prescribed speed of 1.0 m/s and of fast kicking at 2.0 Hz with a speed of 1.5 m/s. They demonstrate the capability of SPH to handle the modelling complexities that human swimming represents.

NOMENCLATURE

c	speed of sound [m/s]
d	swimmer depth [m]
D	drag force [N]
f	kicking frequency [Hz]
Fr	Froude number, $Fr = u_\infty / \sqrt{gL}$
h	kernel smoothing length [m]
L	peak to peak toe amplitude in dolphin kick [m]
p	pressure [N/m ²]
\mathbf{r}	position vector [m]
St	kicking Strouhal number, $St = fL / u_\infty$
t	time [s]
T	kicking period, $T = 1/f$ [s]
u_∞	characteristic free stream/swimmer speed [m/s]
V	maximum characteristic flow speed [m/s]
\mathbf{v}	velocity vector [m/s]
Δp	fluid particle spacing [m]
Δb	boundary particle spacing [m]
μ	dynamic viscosity [Pa s]
ρ	density [kg/m ³]
$\boldsymbol{\omega}$	vorticity, $\boldsymbol{\omega} = \nabla \times \mathbf{v}$ [1/s]

INTRODUCTION

In competitive swimming, participants attempt to complete a set distance in the shortest possible time. Their speed is a function of the complex intertwined factors of active drag forces, propulsive forces, propulsion efficiency and power output (Toussaint and Beek, 1992). A deep understanding of these factors can be

advantageous to determining an individual's optimal stroke technique.

Experimental investigation into the fluid mechanics of human swimming is very difficult because of the highly unsteady nature of the flow and transient deformation of the body of the swimmer. Computational fluid dynamics modelling of human swimming provides non-intrusive access to all spatial and temporal information of the flow field around a swimmer. This allows for improved flow visualisation and understanding of the fluid dynamics. Also, the forces and work across the body surface can be studied and then related to the simultaneous flow structures.

The highest fidelity simulation of human swimming that has been published to date is an immersed boundary large-eddy simulation (LES) of dolphin kick swimming (Mittal et al., 2006; von Loebbecke et al., 2009a, 2009b). Being fully submerged, this did not have the complexity of multiple phases (air and water) and only the relatively minor undulating wave deformation of the body as compared to front crawl. They were able to visualise the generation and propagation of vortices during this stroke and to estimate the mean propulsive efficiency. Bixler et al. (2007) performed a full body simulation of underwater glide swimming using RANS equations in the commercial flow solver Fluent. The force data compared more favourably with their corresponding mannequin towing experiment than with their live human towing experiment. Nakashima et al. (2007) performed simulations of human swimming by prescribing joint motion on a human model composed of truncated cones. Depending on the resultant velocity of each part of the body they estimated forces using simple coefficients gleaned from other simulations and experiments. This means that there was no real simulation of the hydrodynamics. Despite this, Nakashima (2007) was able to analyse the thrust and drag during a cycle of freestyle swimming. This was further broken down by body component, giving insights into the sources of propulsion. Subsequently Nakashima and Motegi (2007) determined the corresponding forces in the muscles during a complete cycle and compared this with electromyography (EMG) muscle data which showed agreement between the activation times of the muscles.

In this paper the SPH numerical method governing equations are first briefly described. Next the process of generating realistic swimmer geometries is outlined and the results from some fixed pose drag tests are presented. The effect of speed on the flow fields is investigated. Then the process for creating realistic swimmer body animation is explored. Finally, the results of underwater dolphin kick simulations are presented and analysed. In this case the

effects of speed and kicking frequency on the flow fields are investigated.

SMOOTHED PARTICLE HYDRODYNAMICS

Smoothed particle hydrodynamics is a Lagrangian mesh-free method for solving partial differential equations. At the heart of this technique is the interpolant (Monaghan, 1992, 1994)

$$A(\mathbf{r}) \approx \sum_{b=1}^n \frac{m_b}{\rho_b} A_b W(\mathbf{r} - \mathbf{r}_b, h), \quad (1)$$

which uses a kernel W and allows for interpolation of randomly scattered points of data. Here m_b is the mass of particle b , ρ_b is its density and A is the quantity to be interpolated. Gradients of scalar quantities may be evaluated using the expression

$$\nabla A(\mathbf{r}) \approx \sum_{b=1}^n \frac{m_b}{\rho_b} A_b \nabla W(\mathbf{r} - \mathbf{r}_b, h), \quad (2)$$

which involves the gradient of the kernel, ∇W . These summations robustly determine the flow quantities and gradients that are used to solve the governing equations. This study utilises the cubic spline kernel with a compact support radius of $2h$ (Monaghan and Lattanzio, 1985).

The Navier-Stokes equations are converted into ordinary differential equation form suitable for the Lagrangian approach of SPH. The domain of interest is filled with approximately equi-spaced particles which can move and change their properties in accordance with the governing equations. The continuity equation is given by

$$\frac{d\rho_a}{dt} = \sum_b m_b \mathbf{v}_{ab} \cdot \nabla W_{ab}, \quad (3)$$

where $\mathbf{v}_{ab} = \mathbf{v}_a - \mathbf{v}_b$ and $W_{ab} = W(\mathbf{r}_a - \mathbf{r}_b, h)$. The form of the conservation of momentum equation is given as (Cleary, 1998)

$$\frac{d\mathbf{v}_a}{dt} = -\sum_b m_b \left[\left(\frac{P_b}{\rho_b^2} + \frac{P_a}{\rho_a^2} \right) - \frac{\xi}{\rho_a \rho_b} \frac{4\mu_a \mu_b}{(\mu_a + \mu_b)} \frac{\mathbf{v}_{ab} \cdot \mathbf{r}_{ab}}{r_{ab}^2 + \eta^2} \right] \nabla_a W_{ab} + \mathbf{g} \quad (4)$$

where the summation is over nearby particles b . If b is a boundary particle then the pressure term is replaced by the boundary force \mathbf{f}_{ak} (see Monaghan (1995b) for details). Here $\mathbf{r}_{ab} = \mathbf{r}_a - \mathbf{r}_b$, \mathbf{g} is the gravitational acceleration, ξ is a constant calibrated for the particular kernel (Cleary, 1998) and η is a small parameter to avoid singularities. More details on the boundary condition modelling and implementation may be found in Monaghan (1995a).

SPH utilises a quasi-compressible approach to avoid having to solve a pressure-Poisson equation at each timestep. Typically the speed of sound is chosen to be ten times the characteristic maximum fluid velocity to ensure the density fluctuations are less than 1% (Monaghan, 1994). The equation of state used in the solver is

$$P = P_0 \left[\left(\frac{\rho}{\rho_0} \right)^\gamma - 1 \right] \quad (5)$$

and the dynamic pressure scale is given by

$$\frac{g}{r_0} \frac{P_0}{\rho_0} = 100 V^2 = c^2. \quad (6)$$

FIXED GLIDE POSE TOWING

We choose our first simulations to be of a swimmer being towed in a fixed glide pose both because data is

readily available for this case and the swimmer can be assumed to be rigid. This has reduced complexity because of the lack of deformation of the body in time.

In a fixed glide pose the human body takes on an outstretched position with arms pointed upwards past the head, the legs straightened and the toes pointed. The hands may be placed one on top of each other or with a small spacing between them. The arms typically press against the ears of the swimmer with head centred between them. In this way both the form area of the swimmer is minimised and a streamlined shape is assumed.

Swimmer geometry and its construction

Swimmer geometries for this investigation were obtained from laser surface scans of athletes which produce unstructured surface meshes of triangles. The female and male meshes used for the fixed glide pose study are given in Figures 1 and 2 respectively. They are both 1.75 m tall (head to heel).

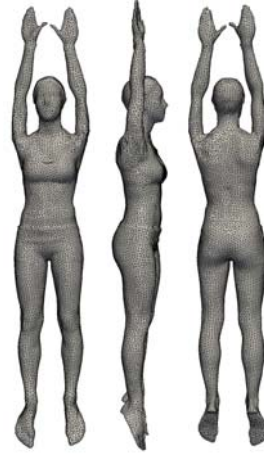


Figure 1: Laser scanned female swimmer mesh in glide pose. Boundary particle spacing is $\Delta b = 20$ mm.

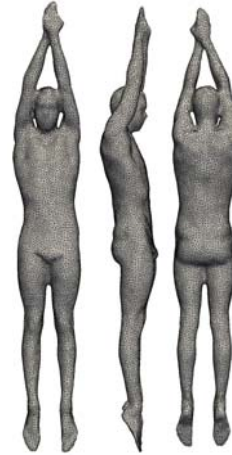


Figure 2: Laser scanned male swimmer mesh in glide pose. Boundary particle spacing is $\Delta b = 20$ mm.

The female swimmer was originally scanned with her arms out to her sides and her feet flat on the floor. Using the animation package Autodesk MAYA, an internal skeletal structure was inserted inside the surface mesh and the mesh was then bound (rigged) to this structure. Subsequent surface mesh deformation may then be performed using linear blend skinning which depends on

nearby joint translations and rotations. The interpolation weightings for difficult regions such as the shoulders had their values manually adjusted to ensure smooth deformations when the arms were stretched upwards. The resultant glide pose produced using this procedure is given in Figure 1. The male swimmer was scanned in the glide pose with his hands together so his arms did not need to be rotated. Because he was physically too tall to fit completely in the scanner, separate scans were made of his upper and lower halves. These were stitched together. His feet were pointed correctly for the glide pose also using the rigging and linear blend skinning procedure.

Fixed glide pose towing simulation results

Simulations of glide pose towing tests were conducted in a 10 m long tank of water which was 2 m deep and 2 m wide. The fluid particle spacing used was 25 mm and the boundary particle spacing of the swimmers was 20 mm. Both the male and female swimmers were towed at speeds of 1.0, 1.5 and 2.0 m/s in the x -direction and at a depth of 0.5 m.

The side-on shape of the human swimmer in a glide pose is somewhat similar to that of a cambered aerofoil. They have similar high aspect ratio shapes which vary in thickness along their lengths first increasing and then decreasing. Aerofoils are known to alternately shed vortices into their wake from their upper and lower surfaces, so similar behaviour may be expected from the swimmer. The three-dimensionality of the real flow is likely to increase the complexity beyond just simple alternating vortex shedding.

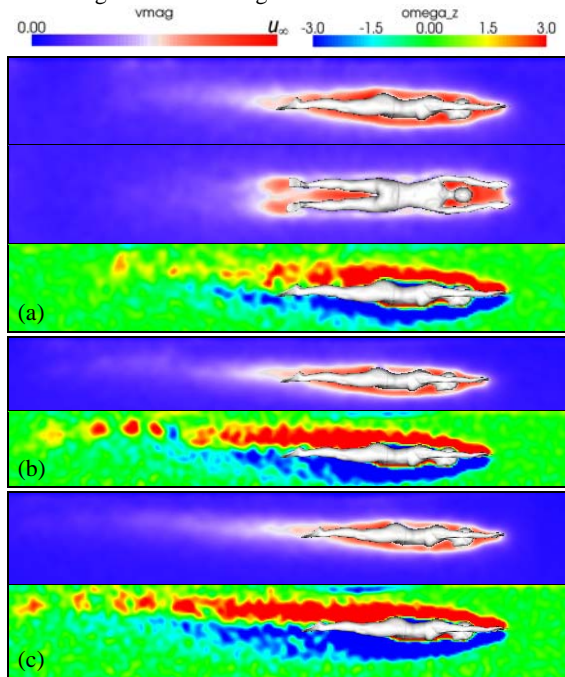


Figure 3: Instantaneous speed and span-wise vorticity of the towed female swimmer in different cross-sections for, (a) $u_\infty = 1.0$ m/s, (b) $u_\infty = 1.5$ m/s, and (c) $u_\infty = 2.0$ m/s.

Figure 3 shows speed and span-wise vorticity of the towed female. Just ahead of the swimmer, the fluid remains in its ambient state, whilst a wake is visible behind. Starting from the hands is a boundary layer sheath of faster moving fluid that is being dragged along with the swimmer. Fluid between the arms and between the legs and close to the top and bottom surfaces moves at speeds

close to that of the swimmer. The speed declines rapidly with distance away from the swimmer's surface. There do not appear to be any large separated flow regions, although flow from the legs divides with a separate wake being shed by each foot. The span-wise vorticity plots highlight the existence of shear layers around the body of the swimmer. Above is a long narrow band of positive vorticity whilst below is matching but somewhat shorter band of negative vorticity. The vorticity pattern in the wake is asymmetric, which is attributable to both the body asymmetry and asymmetry of the water which has a free surface just 0.5 m above.

As the towing speed increases, the velocity distribution remains very similar, but the identifiable wake extends progressively further behind the swimmer. The magnitude of the vorticity also increases and the trail of shed vortices persists for longer.

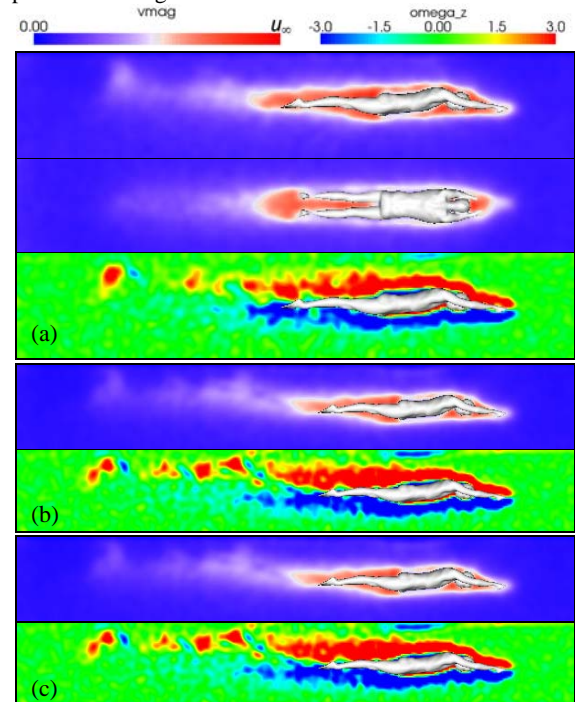


Figure 4: Instantaneous speed and span-wise vorticity of the towed male swimmer in different cross-sections for, (a) $u_\infty = 1.0$ m/s, (b) $u_\infty = 1.5$ m/s, and (c) $u_\infty = 2.0$ m/s.

Figure 4 shows the results from the towing tests of the male swimmer. Many of the same trends are seen as with the female swimmer. The arched shape of the back and neck in this case causes the flow field to be even more asymmetrical. Some of the flow field differences may also be caused by the hands being attached together and the arms pressing against the head, perhaps enabling a more streamlined flow and delaying separation.

Figure 5 shows the predicted drag force as a function of tow speed. The female swimmer experiences a larger drag, most likely because of increased pressure drag from not having her hands together. The drag increases with increasing speed. For a fully submerged object far away from the free surface, drag force would be expected to be proportional to u_∞^2 . However, when near the free surface (as here) additional resistance due to wave drag becomes significant. This has a complex dependence on the Froude number (Fr), leading to a non-quadratic dependence on speed.

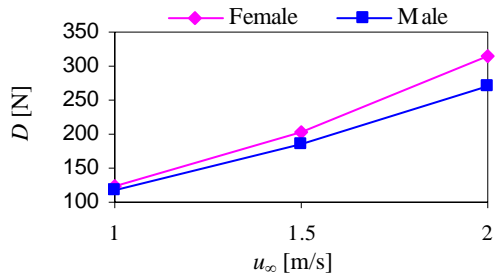


Figure 5: Towing drag force versus speed at 0.5 m depth.

SUBMERGED DOLPHIN KICK SWIMMING

In competitive swimming the submerged dolphin kick is typically used at starts and in turns. This stroke takes advantage of a reduction in wave drag and overall drag that occurs at depth (Vorontsov and Romyantsev, 2000; Vennell et al., 2006). Depending on whether the stroke is freestyle, backstroke or butterfly, the orientation of the stroke may be chosen to be dorsal (face up), ventral (face down) or lateral (sideways). Motion of the body during this stroke is mostly contained within planes parallel to the sagittal plane of the swimmer. When a human performs dolphin kick, the legs kick in unison with the feet pressed together. The body pulses up and down in a wave like motion which passes down along the length of the body towards the feet. The amplitude of this motion increases the further it travels down the body. This stroke is a type of sub-carangiform motion that is similar to the motion of dolphins and other cetaceans.

Swimmer geometry and animation

The swimmer laser scan used for the dolphin kick simulations is shown in Figure 6. This fine resolution scan was re-meshed to create a boundary node spacing of 20 mm.

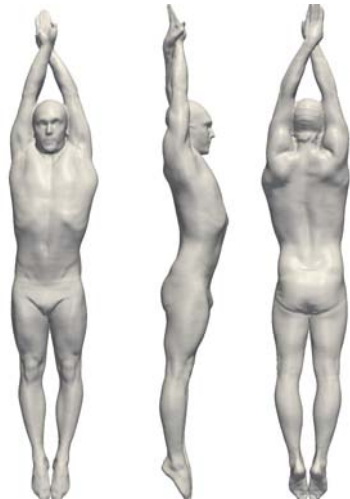


Figure 6: Male laser scan mesh used for the submerged dolphin kick simulations.

In this case the surface mesh was to be animated to closely match one cycle of dolphin kick swimming performed by an elite swimmer. Since the motion is contained almost to a single plane, one side-on angle of swimming footage is sufficient for obtaining full details of the swimming stroke. Joints were carefully inserted into the swimmer mesh and interpolation weightings were assigned. For every frame of the swimmer footage, the

swimmer mesh was placed alongside and adjusted to visually match. An example of such a frame is shown in Figure 7. This adjustment was done by assigning rotations and translations to joints within the swimmer at various times. These joint parameters change smoothly in time by using spline based interpolation. The joint angles in the legs as a function of time are shown in Figure 8 and a corresponding sequence of face-down swimmer frames is shown in Figure 9. The wave-like motion of the torso was achieved by translating the torso joints up and down. It should be noted that the laser scan and the footage come from different individuals.

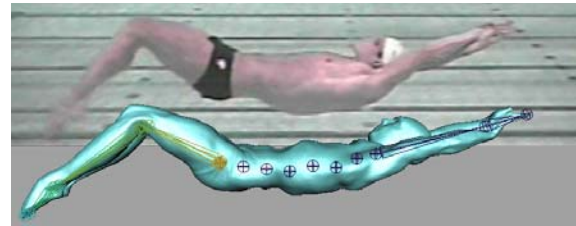


Figure 7: A single pose of the male swimmer model performing dolphin kick along with the corresponding frame of the swimming footage. The internal skeletal structure used to deform the surface mesh is also shown.

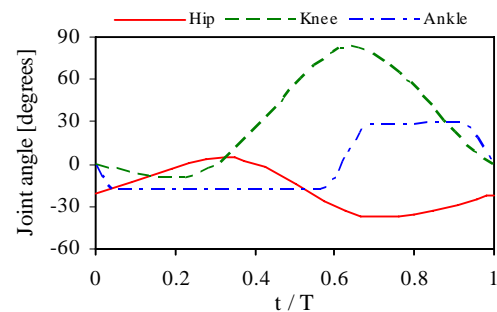


Figure 8: Leg joint angles throughout the dolphin kick swimming cycle. Angles are with respect to the initial pose given in Figure 6.

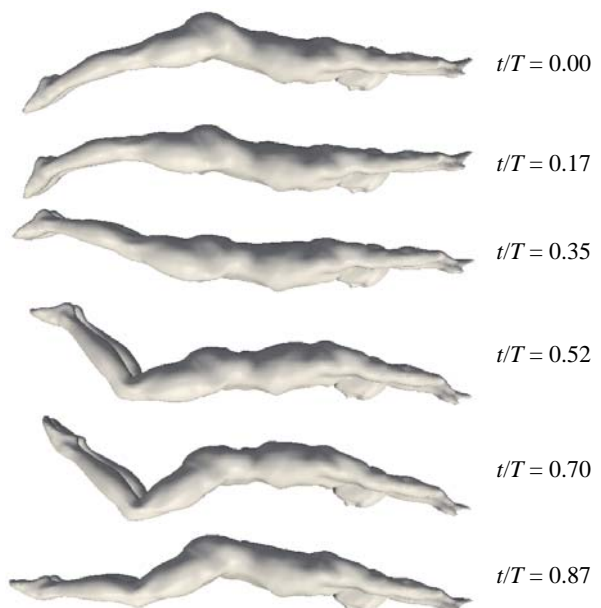


Figure 9: A sequence of frames from the laser scanned male swimmer mesh undergoing dolphin kick swimming.

Submerged dolphin kick swimming simulation results

The dolphin kick animation was exported to a sequence of 37 key-frames covering the kick cycle. In order to ensure smooth surface motion, the solver interpolates nodal positions at intermediate times using the surface nodal velocities supplied along with the key frames. Simulations were again performed in a 10 m long tank which was 2 m deep and 4 m wide with a fluid particle spacing of 25 mm. The cases investigated had kinematics given in Table 1. Case A is a slow kick at 0.8 Hz with a prescribed linear speed of 1.0 m/s. Case B is a fast kick at 2 Hz with a speed of 1.5 m/s. Both used a toe to toe kicking amplitude of $L = 0.50$ m and a depth of $d = 1.0$ m.

Case	T [s]	f [Hz]	u_∞ [m/s]	$St = \frac{fL}{u_\infty}$
A	1.25	0.8	1.0	0.40
B	0.5	2.0	1.5	0.67

Table 1: Dolphin kick kinematics for cases A and B.

Figure 10 shows two snapshots of the velocity magnitude throughout a single kicking cycle for case A. The fluid just ahead of the swimmer is undisturbed whilst there is a clear wake left behind the kicking swimmer. The legs and feet impart significant momentum to the fluid as evidenced by the high velocity contour structures produced from the up and down leg strokes. Figure 11 shows the time evolution of span-wise vorticity for this case. During the knee flexion part of the cycle ($1.83 < t < 2.33$) mostly positive signed vorticity is generated by the feet whilst during the knee extension part of the cycle ($2.33 < t < 2.83$) weaker negative signed vorticity is produced in the fluid. These vortices tend to move slowly away from where they are shed whilst the swimmer continues moving forwards. Similarly Figure 12 shows the time evolution of vorticity for the fast kicking case B. Vorticity generation is stronger in this case due to the faster kicking speed of the legs. The sequence of oppositely signed vortices behind the swimmer is much clearer. They are reminiscent of a Karman vortex street despite being generated by forced oscillation of the feet instead of flow over a bluff body.

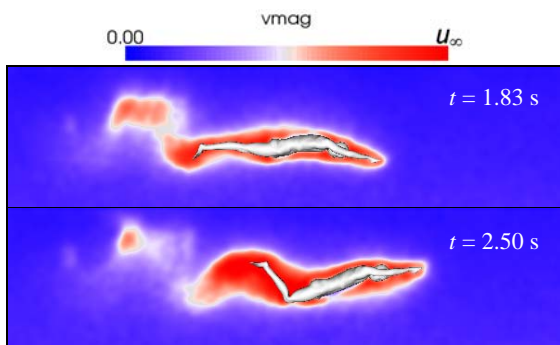


Figure 10: Instantaneous speed throughout a single dolphin kick cycle for case A in the $z = 0$ (sagittal) plane.

Cases A and B used the same swimming kinematics and differed only in the parameters of kicking frequency and swimmer speed. The wake structures behind the swimmer in both cases were dominated by the forcing supplied by the body rather than from any natural vortex shedding. In dolphin kick swimming most of the propulsive force is caused by the legs and feet which at

some stage produce a thrust generating jet of fluid (von Loebbecke et al, 2009a). It is difficult to discern this in the present results and further investigation is required.

Figure 13 shows instantaneous isosurfaces of vorticity in the fluid, demonstrating the strong three-dimensionality of this flow around a moving swimmer. The vortical structures shed into the wake are of finite span-wise length. Each limb sheds vortices that are initially distinct but merge further downstream.

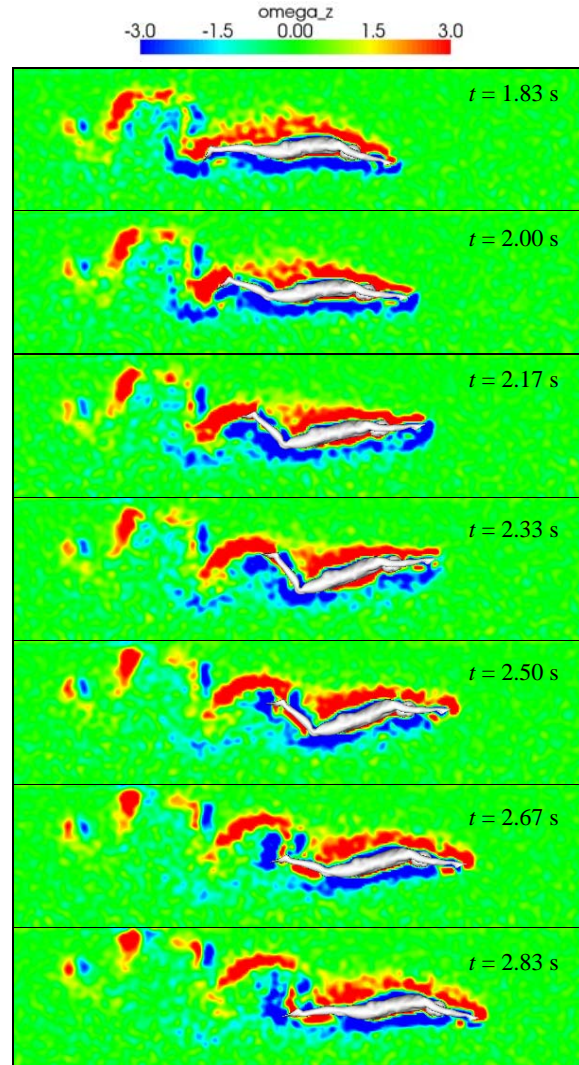


Figure 11: Instantaneous span-wise vorticity contours (ω_z) on the $z = 0$ (sagittal) plane throughout a single dolphin kick cycle for case A.

CONCLUSIONS

This paper has demonstrated the suitability of the SPH technique to model the highly challenging problem of human swimming. The main difficulties in such an application are due to free surfaces and highly complex deforming geometry.

The fixed glide pose towing tests at different speeds showed realistic trends in the drag forces and in the qualitative appearance of the flow fields. It is reported in the literature that the overall drag on a passively towed human swimmer in glide pose is larger near the surface due to wave drag (Vennell et al., 2006). SPH is capable of

modelling surface waves so the effects of depth will be investigated soon.

The modelling of the complex geometry of the swimmer surface is handled effectively using laser scanning, swimming footage and a commercial animation package. The SPH solver is able to utilise the resultant unstructured deforming mesh as a boundary condition.

The submerged dolphin kick simulations display realistic flow fields around the swimmer, despite the fluid resolution coarseness. With encouragement from these results, high resolution cases will be run in the future.

Ultimately this computational approach will allow a more scientific understanding and evaluation of different swimming strokes, leading to improved techniques and performance.

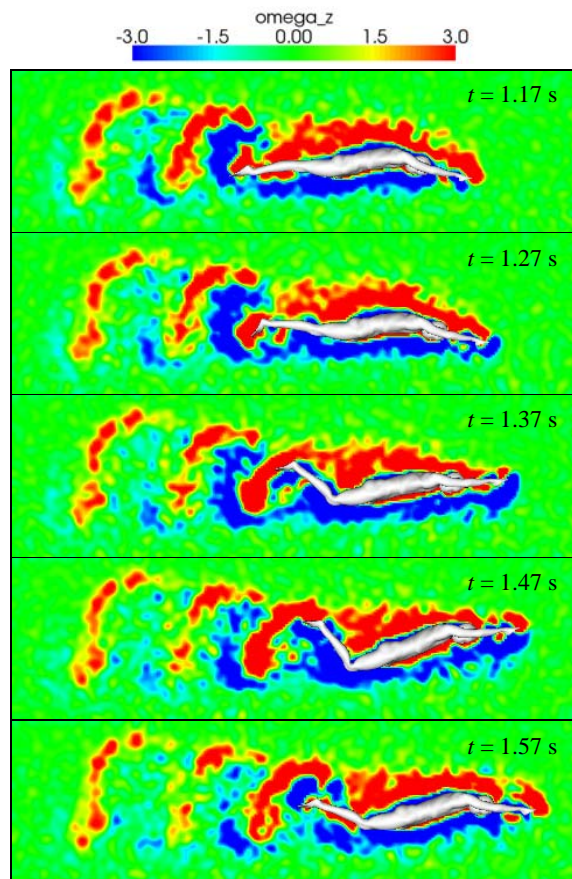


Figure 12: Instantaneous span-wise vorticity contours (ω_z) on the $z = 0$ (sagittal) plane throughout a single dolphin kick cycle for case B.

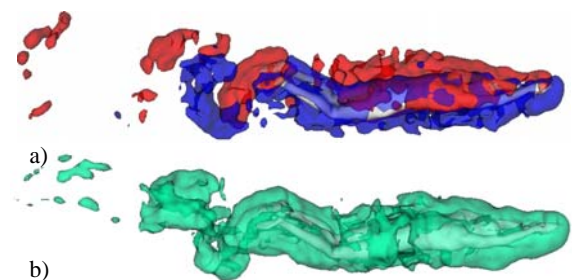


Figure 13: Instantaneous isosurfaces in the fluid around the swimmer performing dolphin kick at $t = 1.37$ s for case B. (a) $\omega_z = 3$ is red and $\omega_z = -3$ is blue, and (b) $|\omega| = 5$.

REFERENCES

- BIXLER, B., PEASE, D. and FAIRHURST, F., (2007), "The accuracy of computational fluid dynamics analysis of the passive drag of a male swimmer", *Sports Biomech.*, **6**, 81-98.
- CLEARY, P. W., (1998), "Modelling confined multi-material heat and mass flows using SPH", *Appl. Math. Model.*, **22**, 981-993.
- MITTAL, R., DONG, D., BOZKURTAS, M. and VON LOEBBECKE, A., (2006), "Analysis of Flying and Swimming in Nature Using an Immersed Boundary Method", 36th AIAA Fluid Dynamics Conference and Exhibit, San Francisco, California.
- MONAGHAN, J. J. (1992), "Smoothed Particle Hydrodynamics", *Annu. Rev. Astron. Astrophys.*, **30**, 543-574.
- MONAGHAN, J. J., (1994), "Simulating free surface flows with SPH", *J. Comput. Phys.*, **110**, 399-406.
- MONAGHAN, J. J. (1995a), "Improved modelling of boundaries", SPH Tech. Note #2, CSIRO Div. of Maths and Stats, Tech. Report DMS-C 95/86.
- MONAGHAN, J. J. (1995b), "Simulating gravity currents with SPH: III Boundary Forces", *Rep. 95/11*, Department of Mathematics, Monash University, Melbourne, Australia.
- MONAGHAN, J. J. and LATTANZIO, J. C., (1985), "A refined particle method for astrophysical problems", *Astron. Astrophys.*, **149**, 135-143.
- NAKASHIMA, M., (2007) "Mechanical Study of Standard Six Beat Front Crawl Swimming by Using Swimming Human Simulation Model", *J. Fluid Science and Tech.*, **2**, 290-301.
- NAKASHIMA, M. and MOTEGI, Y., (2007), "Development of a full-body musculo-skeletal simulator for swimming", Proc. of the 2007 Int. Symp. on Computer Simulation in Biomechanics (ISCSB2007), 59-60.
- NAKASHIMA, M., SATOU, K. and MIURA, Y., (2007) "Development of Swimming Human Simulation Model Considering Rigid Body Dynamics and Unsteady Fluid Force for Whole Body", *J. Fluid Science and Tech.*, **2**, 55-67.
- TOUSSAINT, H. M. and BEEK, P. J., (1992), "Biomechanics of competitive front crawl swimming", *Sports Med.*, **13**, 8-24.
- VENNELL, R., PEASE, D. and WILSON, B., (2006), "Wave drag on human swimmers", *J. Biomech.*, **39**, 664-671.
- VON LOEBBECKE, A., MITTAL, R., MARK, R. and HAHN, J., (2009a), "A computational method for analysis of underwater dolphin kick hydrodynamics in human swimming", *Sports Biomech.*, **8**, 60-77.
- VON LOEBBECKE, A., MITTAL, R., FISH, F. and MARK, R., (2009b), "Propulsive Efficiency of the Underwater Dolphin Kick in Humans", *J. Biomech. Eng.*, **131**.
- VORONTSOV, A. R. and RUMYANTSEV, V. A., (2000), "Resistive forces in swimming," In: Zatsiorsky, V. (Ed.), "Biomechanics in Sports: Performance Enhancement and Injury Prevention. Vol. IX. Encyclopaedia of Sports Medicine." Blackwell, IOC Medical Commission, Ch. 9.